

Kilometer-range nonlinear propagation of femtosecond laser pulses

Miguel Rodriguez,¹ Riad Bourayou,^{1,2} Guillaume Méjean,³ Jérôme Kasparian,^{3,*} Jin Yu,³ Estelle Salmon,³ Alexander Scholz,⁴ Bringfried Stecklum,⁴ Jochen Eislöffel,⁴ Uwe Laux,⁴ Artie P. Hatzes,⁴ Roland Sauerbrey,² Ludger Wöste,¹ and Jean-Pierre Wolf³

¹*Teramobile, Institut für Experimentalphysik, Freie Universität Berlin, Arnimallee 14, D-14195 Berlin, Germany*

²*Teramobile, Institut für Optik und Quantenelektronik, Friedrich-Schiller-Universität Jena, Max-Wien-Platz 1, D-07743 Jena, Germany*

³*Teramobile, LASIM, UMR CNRS 5579, Université Claude Bernard Lyon 1, 43 boulevard du 11 Novembre 1918, F-69622 Villeurbanne Cedex, France*

⁴*Thüringer Landessternwarte Tautenburg (TLS), Karl-Schwarzschild-Observatorium, Sternwarte 5, D-07778 Tautenburg, Germany*

(Received 30 September 2003; published 30 March 2004)

Ultrashort, high-power laser pulses propagating vertically in the atmosphere have been observed over more than 20 km using an imaging 2-m astronomical telescope. This direct observation in several wavelength bands shows indications for filament formation at distances as far as 2 km in the atmosphere. Moreover, the beam divergence at 5 km altitude is smaller than expected, bearing evidence for whole-beam parallelization about the nonlinear focus. We discuss implications for white-light Lidar applications.

DOI: 10.1103/PhysRevE.69.036607

PACS number(s): 42.68.Wt, 42.68.Ay, 42.65.Jx, 42.65.Re

INTRODUCTION

High-power ultrashort (femtosecond) laser pulses propagate in air in a self-guided mode due to a dynamic balance between Kerr-lens focusing and defocusing on laser-induced plasma [1]. This results in a breakup of the beam in one or several filaments of about 100 μm in diameter that propagate over distances much longer than the Rayleigh length. Each filament contains a very high, quasiconstant, intensity of typically 10^{14} W/cm² [2,3], which allows efficient self-phase modulation and generation of a broadband white-light continuum spanning from the UV [4] to the mid-IR [5].

These properties open exciting perspectives for applications [6] such as white-light Lidar (light detection and ranging) [7,8] and laser lightning control [9,10]. These applications in turn stimulate the need for a better characterization of the filament formation over atmospheric scales, i.e., in the km range. In particular, the filaments onset and length are key parameters for spectroscopic measurements of atmospheric compounds and for depositing the desired intensities on remote targets. Wille *et al.* [11] have shown that the filament location strongly depends on the peak power and initial chirp. A negative chirp (i.e., launching the blue part of the spectrum before the red part) can be used to compensate group-velocity dispersion (GVD) in air, and thus to select the distance at which the Fourier components will recombine, leading to high intensity. Together with spatial focusing using a sending telescope, this “temporal focusing” allows us to select the distance at which filamentation will start. Filamentation lengths up to 200 m have been reported by La Fontaine *et al.* [12] on a horizontal optical path. Conversely, in vertical propagation, Rairoux *et al.* [7] have detected white light from altitudes as high as 13 km, but without evidence that the continuum was generated at that altitude rather than near to the ground, with subsequent linear propagation and elastic backscattering.

Vertical propagation is of particular interest because (1) the gradients in pressure and temperature with altitude modify the nonlinear propagation process [13] and (2) most of the atmospheric applications such as Lidar profiling and lightning control require a vertical laser emission. However, characterizing vertical propagation at high altitude is a difficult task because the strong nonlinearity of the problem prevents extrapolation from experimental results at short distances and/or reduced peak powers. Moreover, most numerical simulations [14,15,16] require unreasonable times to get insight in the km-range propagation. First theoretical results about propagation over kilometer-range distances have been reported recently, predicting an overall collapse of the pulse above 20 km altitude under adequate laser parameters [17]. However, this long-distance result was obtained at the cost of a simplified variational calculation, illustrating how difficult exact long-distance propagation simulations are. Propagation experiments at long distance are needed to validate such emerging numerical simulations, and to develop simpler models allowing reasonable computing times usable for applications. The current filament characterization techniques are based on filament conductivity [18,19], nitrogen fluorescence [20], sonometry [21], or terahertz radiation [22], which are local measurements, and thus unpractical for very-long distance measurements, especially in the vertical direction.

In this paper, we investigate the vertical propagation of ultrashort, high-power laser pulses over more than 20 km in the atmosphere. Spectral as well as geometrical data have been acquired using a large scale (2 m) imaging telescope and permit us to fully characterize the beam geometry, showing evidence of anomalous beam propagation on km scales. These measurements constitute a data set for nonlinear propagation in a gaseous medium with (known) decreasing pressure and temperature gradients. Moreover, the white-light generation at high altitudes is investigated as a function of the laser parameters, especially chirp and initial focusing. These data are used for the optimization of white-light Lidar configurations.

*Email address: jkaspari@lasim.univ-lyon1.fr

EXPERIMENTAL SETUP

Experiments were performed using the Teramobile system as ultrashort laser source. This mobile femtosecond laser system is described in detail elsewhere [11]. Briefly, it consists of a Ti:sapphire oscillator and CPA amplification chain integrated in a mobile laboratory. It also includes a full Lidar detection equipment. The Teramobile laser provides 100 fs pulses with a peak power of 3 TW in the near infrared (800 nm), at a repetition rate of 10 Hz. In most of the experiments, the laser beam was emitted vertically as a parallel beam with a typical $1/e^2$ diameter of 3 cm. However, in some of the experiments, an off-axis sending telescope with a tunable focal length was used to expand the beam by a factor of 3, and focus it, with an adjustable focal length. In addition to focusing and initial diameter, the initial laser chirp was varied during the experiments by moving a grating in the compressor. Three chirp values have been used: a short pulse with slight GVD precompensation (150 fs pulse duration), as well as long pulses with strong GVD precompensation and anticompensation (both with 600 fs pulse duration). The focus and chirp changes did not alter the alignment of the laser beam, which remained vertical within ± 0.3 mrad along the whole experiment.

The Teramobile system was installed at a distance of 30 m from the $f=4$ m, 2-m diameter telescope [23] of the Thüringer Landessternwarte (Thuringian State Observatory/TLS) in Tautenburg (Germany), used in its Schmidt (imaging) configuration. The imaging device was a CCD with 2048×2048 pixels, providing an angular resolution of $6 \mu\text{rad}$ /pixel. The sensitivity range of the CCD is 350 to 1000 nm. Integration times between 1 s and 1 h have been used, although typical exposure times ranged between 1 and 360 s. The good linearity of the 16-bit CCD camera allowed us to intercalibrate the relative intensity between images with different integration times.

The slightly off-axis position of the Teramobile, 30 m away from the telescope, allowed both (i) cross-section images of the beam on the bottom of clouds or haze layers acting as screens and (ii) side imaging of the Rayleigh-scattered light from the beam over large altitude ranges (Fig. 1). In the latter case, the precise altitude was retrieved using adequate triangulation. This range was cross checked by precise classical Lidar measurements of the cloud height in the near-IR channel. The astronomical telescope is always focused to infinity, generating a blur on the images, especially at low altitudes. When using the images to retrieve the beam divergence, the beam profiles measured are deconvolved with the blur function of the telescope at the considered distance.

Images have been taken with several glass filter sets (Table I), covering the visible and infrared sides of the white-light continuum, as well as the fundamental wavelength. To take into account the high dynamics of the white-light spectrum [5], the contribution of the fundamental to the overall signal going through each filter is estimated, based on an integration of the spectrum previously measured in the laboratory [5]. Filters B and BG, which have rejections of better

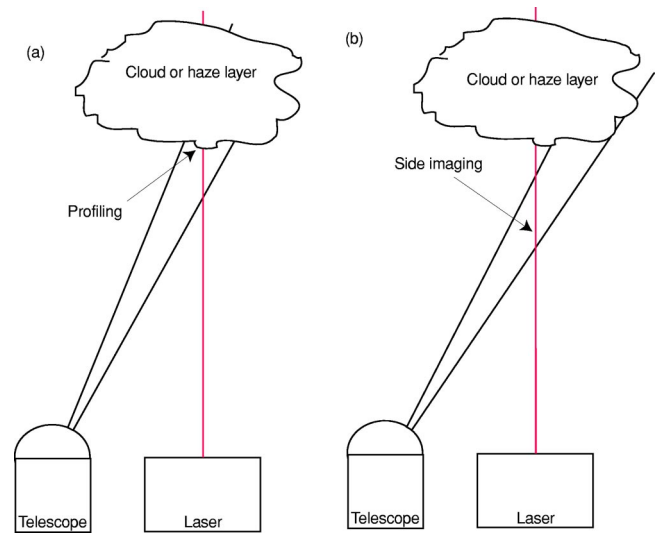


FIG. 1. (Color online) Principle of beam imaging. (a) Beam profiling on a cloud or haze layer. (b) Side imaging of the beam with Rayleigh scattering. In real pictures (see also Fig. 3), a combination of both components is visible together.

than 10^{-15} around 800 nm, block the fundamental completely.

RESULTS AND DISCUSSION

Nonlinear propagation and filamentation

Nonlinear propagation and filamentation of ultrashort lasers in air have recently been studied both theoretically [15,24,25] and experimentally [26,27,28]. However, most of the studies were limited to short distance (up to some tens of m) and/or low pulse energy. When the laser pulse power is of the order of the critical power $P_c \approx 3$ GW [29] the beam forms a single filament of typically $100 \mu\text{m}$ in diameter, which can propagate over several meters. 10–20% of the total pulse energy (i.e., a few mJ) is then localized in the filamentary structure [30], while the rest of the energy remains in the surrounding unfocused beam that propagates with it. This surrounding “energy reservoir” dynamically feeds the filament [16,30] and allows it to propagate over long distances. The high intensity inside the filament (10^{14} W/cm²) generates new frequencies in the laser spectrum by self-phase modulation (SPM), leading to a broad supercontinuum [Fig. 2(a)]. Part of this supercontinuum is, however, emitted in a narrow cone around the filament. The angle of this conical emission decreases with wavelength, contrary to usual diffraction [26,31,32].

When the laser pulse power reaches several $10\text{--}100P_c$, as is the case for TW lasers, the beam breaks up in many “cells,” which each contain about the critical power and generates a filament. The whole beam is formed of a large number of filaments, interacting with a surrounding “photon bath” containing the rest of the pulse energy. It has been predicted numerically that the beam as a whole, including the photon bath, propagates nonlinearly, with a turbulent energy exchange between permanently nucleating and dying filaments and the photon bath itself [16]. Figure 2(b) shows

TABLE I. Filters used.

Symbol	Filter	Wavelength range (combined with CCD efficiency, nm)		Contribution of the fundamental wavelength to the overall transmitted signal	Description
		10% of T_{\max}	50% of T_{\max}		
B	Johnson B+BG39, 8+2 mm	370–510	390–480		Blue white light
BG	BG39, 3 mm	340–610	370–580		Visible (green) white light
I	Johnson I, 8 mm	750–1000	770–950	50%	Fundamental wavelength
RG	RG850, 3 mm	830–1000	840–970	15%	IR white light

an experimental cross section of such a TW laser beam, after 15 m propagation. In this picture, an IR filter has been used to cut off the white-light continuum generated by each filament. Light emission from the different filaments has been found to be coherent [33]. Recent high-level three-dimensional (3D) [34] and 4D calculations (3D+time) [16] have been able to successfully simulate this behavior over ten to several tens of meters. Numerical instability related to the high nonlinearity of the nonlinear Schrödinger equation prevented simulations over longer distances. The propagation over longer (km-range) distances, and related questions such as (1) the filamentation length, (2) the propagation characteristics (e.g., divergence) of the whole beam including photon bath, and (3) the effect of pressure and temperature gradients are unknown so far.

Long-distance–high-resolution imaging of nonlinearly propagating TW lasers

Figure 3(a) displays a typical image in the fundamental wavelength channel of the femtosecond-TW laser beam, emitted as an initially parallel beam with 3 cm diameter. Elastic scattering is detected from the ground to an altitude of at least 25 km (integration time of 1 s). Similar measurements in the white-light band [BG filter, Fig. 3(b)] demonstrate efficient supercontinuum generation by SPM. Under haze-free conditions, white-light signals in the blue region (B filter) have been detected from altitudes beyond 18 km (exposure time of 360 s).

The image of the beam impact on the bottom boundary of the aerosol layer (e.g., cirrus clouds) can be seen as a remote

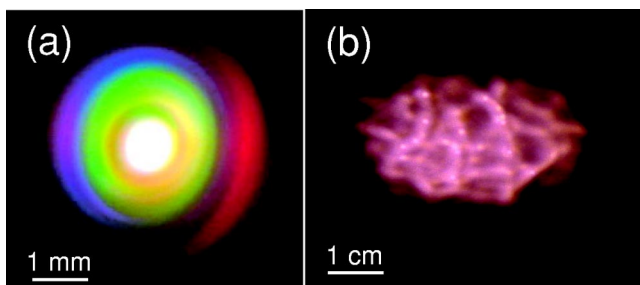


FIG. 2. (Color online) (a) Conical emission from a femtosecond laser beam in air, near to the critical power P_{cr} . (b) Beam profile of a high-power beam ($1000 P_{\text{cr}}$) after 15 m propagation. Multiple filamentation is clearly visible.

beam profiler. The depth of this nonopaque screen can lead to some slight image distortion and it decreases the image resolution. With higher aerosol density, multiple scattering induces some errors in the profile and affects the image resolution too. In our conditions, numerical simulations showed that the multiple scattering contribution distorts the beam profile on the cloud by less than 10%. Fluctuations due to cloud inhomogeneity are mainly smoothed out by time averaging. An example of such a remote profile of an initially focused ($f=25$ m) beam, measured in the RG band (near infrared), is shown in Fig. 4. In this profile, taken from a cloud at an altitude of 9.6 km, a structure with two maxima is clearly visible. It is very interesting to notice that although the beam experienced nonlinear propagation and filamentation at lower altitude, this remote profile reflects the initial profile of the beam, which also exhibited a two-peaks mode (see inset). The beam seems therefore to keep a long term memory of its initial characteristics, which survived nonlinearity and modulational instability. Two key parameters are used to control the non-linear propagation and filamentation processes: temporal focusing (impinging an initial chirp to the pulse) and spatial focusing using the variable focal length sending telescope.

Filamentation altitude and control by temporal focusing

Beam profile images have been taken on a cloud at 6 km altitude in the white-light *B* band. The beam is sent parallel and with a very low GVD precompensation (corresponding to an initial duration of 150 fs of the launched pulse). The observed images on the cloud exhibit a ring structure around the laser beam, with a diameter of 32 m and a typical ring width of 6 m [Fig. 5(a)]. This ring is clearly the projection of conical emission from the filaments formed at lower altitudes. This allows us to estimate the altitude at which filamentation ends. In our case, the ring structure on the cloud leads to an half angle from ground of about 2.7 mrad and a ring width of 1 mrad. As this angle is typical for the angle of conical emission in this spectral region [27,31,32], we can conclude that the filaments are generated (and end) close to the ground level [see Fig. 5(b)]. This is consistent with previous short distance horizontal measurements, where filamentation started at 8 m and ended at 35 m from the system for a parallel beam with similar chirp configuration [11].

Figure 5(c) shows a transversal cut of the beam profile intensity [horizontal, passing through the maximum in Fig.

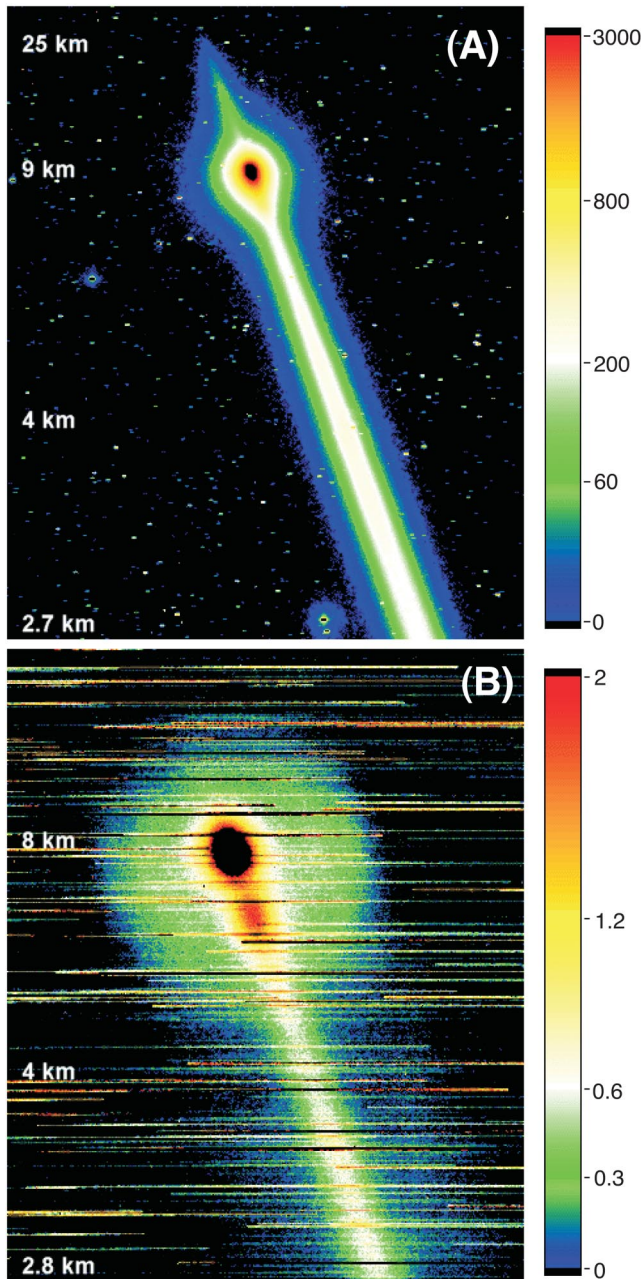


FIG. 3. (Color online) Typical fs beam image taken with the CCD camera of the Tautenburg observatory. (a) Fundamental wavelength, 1 s exposure time, (b) in the BG band, 180 s. The color scales indicate the signal intensities, normalized to the exposure time. The horizontal strips across the pictures are stars passing through the telescope field of view. Note the strongly nonlinear altitude scale due to triangulation. Both images correspond to slight GVD precompensation.

5(a)]. This curve can easily be reproduced by a simulated beam profile, calculated as follows. The white-light is assumed to have a flat wavelength dependence within the transmission window of the B filter. Hence, the measured spectrum is the transmission curve of the B filter. On the other hand, the wavelength dependence of the conical emission from the literature [27,31,32], can be seen as an inverse dispersion relationship, which, combined with the spectrum,

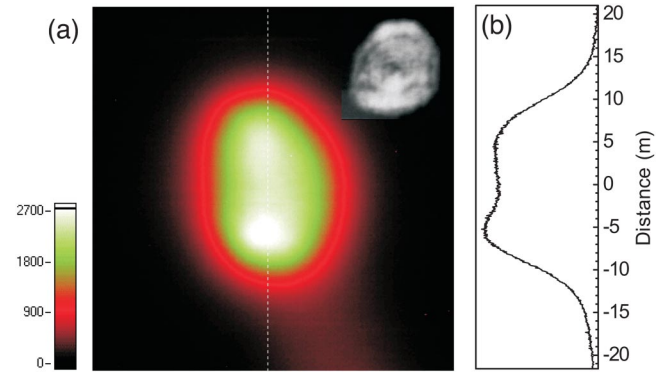


FIG. 4. (Color online) (a) Beam profile on an aerosol layer (thin cirrus) at 9.6 km altitude, showing a double structure in the beam (after focusing with $f=25$ m). Inset: initial beam profile. (b) Intensity cut across the dotted line of image (a).

yields a spatial profile of the conical emission. Once superimposed with the central peak, this simulated beam profile fits the experimental one very well. Note that the lower contrast of the experimental data is due to the unsharpness of the image.

Radially integrating the simulated curve allows us to estimate that the ring structure accounts for 65% of the overall white-light energy in this band. This is the first time, to our knowledge, that the amount of white light emitted into the conical emission by long filaments has been estimated. Also notice that in our multifilamentation case, the observed conical emission is generated by the overlap of the conical emission of many filaments, forming a bundle inside the main laser beam, as shown above in Fig. 2(b).

A second set of images has been obtained using an initial negative chirp, corresponding to 600 fs pulse duration, to compensate GVD on longer distances. In this case the rings merge to the central peak, forming a narrow pedestal [Fig. 5(d)]. Considering that the initial chirp of the pulse does not affect the angle of conical emission [31], this reduced projected radius of conical emission is the signature for an emission occurring nearer to the cloud, i.e., at higher altitude [Fig. 5(e)]. The height of the conical emission has been fitted from the experimental curves, and amounts to $2 \text{ km} \pm 0.5 \text{ km}$. The uncertainty on the measurement is mainly due to the narrowness of the pedestal.

The same altitude change with chirp has been confirmed by results in the blue-green spectral region (BG filter). An independent estimation based on the reduction of the diameter of the central peak of the beam profile, as imaged on high-altitude clouds, also yield filaments in the range of 2 km altitude when GVD is adequately compensated. These estimations provide the first evidence, to our knowledge, of filamentation at km-range altitudes.

Beam divergence and spatial focusing effects

Outside the aerosol layers, Rayleigh scattering provides a side image of the beam. This allowed us to measure the divergence of the whole beam (which contains the filament bundle and the photon bath) by measuring its cross-section dimension as a function of altitude. Divergence measure-

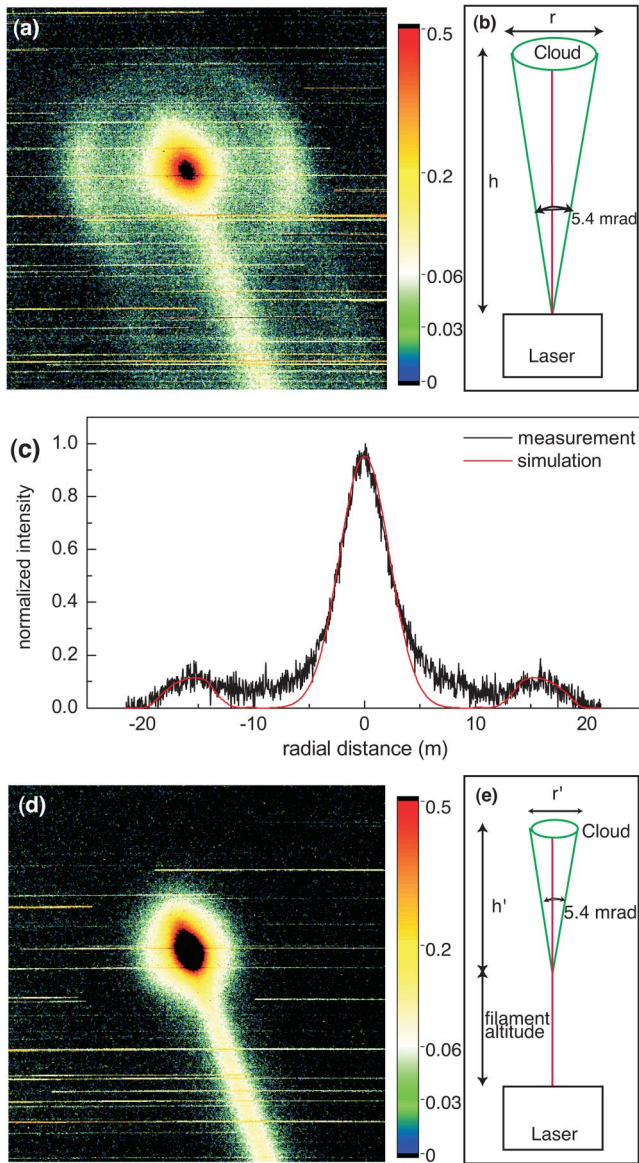


FIG. 5. (Color online) (a) Beam impact on a haze layer and cut across the impact, in the blue (B) band of the white light, with slight GVD precompensation. The conical emission ring is clearly visible. (b) Schematic of the ring emitted from low-altitude filaments imaged on high-altitude clouds. (c) Cross section profile through the intensity maximum of the image (a), and simulation of conical emission (for details see text). (d), (e) Same as (a) and (b) for a stronger GVD precompensation, pushing the filamentation to higher altitudes, and reducing the apparent diameter of the imaged conical emission.

ments were performed for both the fundamental wavelength and the white-light continuum.

By sweeping the telescope vertically along the beam and assembling eight images, we were able to determine the beam size from 600 m to 20 km altitude. For the first measurement of the beam divergence at the fundamental wavelength (I filter), the beam was sent parallel and with a slight GVD precompensation corresponding to an initial pulse duration of 150 fs. The beam divergence is found to be almost constant over the whole altitude range with a value of 0.16

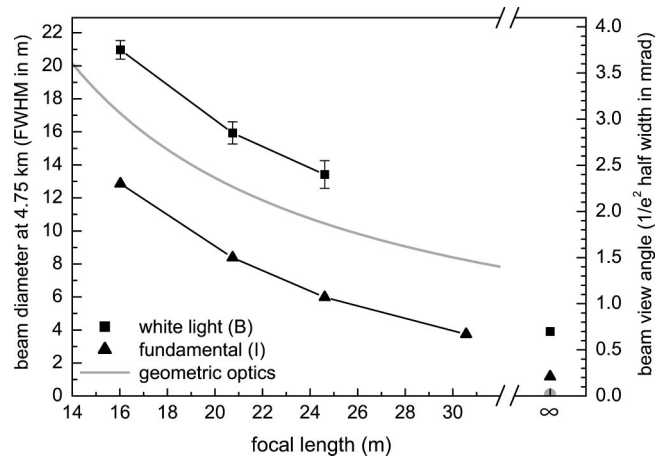


FIG. 6. Focus dependence of the beam divergence for filters B and I at 4.8 km altitude, with slight GVD precompensation. Both vertical scales (left: FWHM in meter, right: $1/e^2$ half angle in mrad) are valid for all the points. The error bars in the range of the symbol sizes have been omitted. For infinite focal length, the gray dot indicates the diffraction limit.

mrad (half angle at $1/e^2$), three times the specified divergence of the laser output.

No significant effect on the whole fundamental wavelength beam divergence was observed by changing the initial chirp settings. We evaluated the effect of initial spatial focusing, by varying the transmitter focal length from 16 to 30 m. The results are summarized in Fig. 6. The divergence of the beam at 800 nm steadily decreases with focal length from 2.3 mrad to 0.6 mrad, respectively. Geometric optics predicts that the respective opening angle (divergence) after focus (see the gray line in Fig. 6) is significantly larger than the observed divergence. The difference between the two curves is almost constant and amounts to 0.6 mrad. This is the signature for an overall nonlinear parallelization of the whole beam near the focus, showing evidence for a nonlinear propagation not only of the filaments, but of the beam as a whole, as predicted by Mlejnek *et al.* [16]. However, no further anomalous divergence of the beam as a whole was observed at high altitude (measured up to 18 km), as was, for example, predicted theoretically by Sprangle *et al.* [17]. Their simulation yields a collapse of the whole beam around 20 km altitude. However, their simulations are not directly comparable to our experimental results since they use longer, slightly focused pulses with much lower peak power, resulting in predicted self-focusing lengths in the 100-km range.

Divergence measurements were also performed for the white-light supercontinuum generated by SPM. When the beam is sent parallel, the white light contained in the whole beam is significantly more divergent than the fundamental, e.g., 0.7 mrad in the B band instead of 0.16 mrad. This value is larger than a diffraction-limited behavior of the whole 3 cm beam, but still much smaller than would be expected from diffraction at the exit of a commonly considered 100 μm filament. This suggests that the filaments vanish gradually, with their diameter increasing up to about 300 μm near their end, where the white light is released. Note that such a large diameter was observed by Lange *et al.* in a gas cell

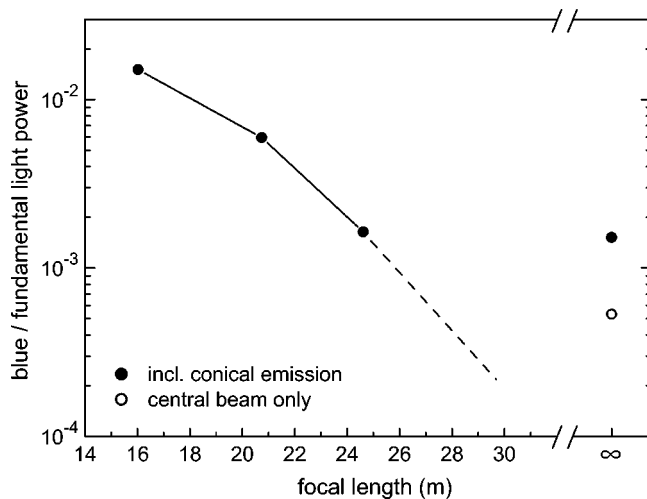


FIG. 7. Conversion efficiency at 4.8 km of the ultrashort pulses into the blue (B) band of the white-light continuum, as a function of focus. Note that the collimated beam (infinite focal length) has a smaller diameter than focused ones (3 cm instead of 10–12 cm), resulting in a more intense white-light generation. The signal for $f=30$ m lies below detection limit, which amounts to 2×10^{-4} .

[35]. The small divergence of the white light might also be related to a recollimation by the Kerr effect after it exits the filament, or to multiple filaments acting as several coherent, in-phase point sources interfering to generate a narrow emission lobe. Anyway, this small divergence of the white light is favorable in view of Lidar applications, since the 0.7 mrad (half angle) value is in the same range or smaller than the field of view of typical Lidar receivers. This relatively collimated emission is consistent with the fact that the supercontinuum consists of coherent light [33].

The white-light divergence has also been measured as a function of the initial beam focusing (Fig. 6). It was derived in the blue band (B filter set) from the beam diameter on images far beyond the geometrical focus (at 4750 m distance). The white light is, again, more divergent than the fundamental wavelength. Its divergence is equal to that of conical emission from a single filament [27,31,32], convoluted with the divergence of the fundamental beam. This behavior is consistent with the idea that the white light is emitted by each filament with the same angular distribution as from single filaments, while the divergence of the filament bundle itself is imposed by the initial focusing.

White-light generation efficiency

In view of Lidar applications, the white-light generation efficiency is a key parameter. We have systematically studied the influence of GVD precompensation (chirp) and of the initial beam focusing on the white light conversion efficiency in the visible range at a remote location (4750 m altitude). We used I as the fundamental wavelength band and B as the white-light indicator. The intensity was estimated from a transverse integration of the beam profile on the haze layer. Figure 7 displays this white-light conversion efficiency into the B band as a function of the initial beam focus. Obviously, strong focusing yields more efficient white-light generation,

up to a factor of 50 compared to an initially parallel beam. Note that, in our experiment, the diameter of the parallel beam is 3 times smaller than the focused beam. This increases the incident intensity, causing stronger SPM and more filaments than for slightly focused beams with a larger initial diameter.

The effect of chirp was investigated by comparing the white-light generation efficiency of the unfocused laser into the BG band, for pulses with 600 fs initial pulse duration, but opposite chirps. The conversion efficiency is at least 6 times more efficient when the initial chirp compensates the GVD, than for GVD anticompensation. In the B band the factor seems to be larger, although it could not be measured precisely.

The above results show that the nonlinear process can be controlled and optimized by adjusting the initial chirp and focus of the laser beam. Even for the shortest focal lengths used, the white-light divergence is smaller than the typical Lidar receiver field of view (several mrad), which allows us to take benefit of the much higher conversion efficiency into the white light. Note that this behavior was actually observed in the UV [36]. Further investigation is required, however, to determine the optimal focus, which would correspond to a white-light divergence comparable to the Lidar receiver field of view.

CONCLUSION

As a conclusion, direct imaging observation of femto-second-terawatt laser pulses propagating in the atmosphere have shown evidence for remote nonlinear propagation of high-power ultrashort laser pulses in the atmosphere. Especially, we observed a nonlinear behavior of the beam as a whole [16], since the whole laser beam is partly recollimated near the nonlinear focus and filamentation occurs up to 2 km altitude. The focus dependence of the white-light generation efficiency and divergence yields indications for the optimization of white-light Lidar signals.

Remote imaging gives access to long-range observation of the nonlinear propagation of ultraintense laser beams as shown in this work, e.g., with the analysis of conical emission. Further work is required to characterize the propagation at medium-range distances, typically between 500 m and 5 km. Especially, *in situ* measurements would adequately complement our remote analysis. Moreover, extension of our results to the infrared side of the white-light continuum would allow us to compare the processes at play in its generation on both sides of the fundamental wavelength and the corresponding parameters for Lidar optimization.

ACKNOWLEDGMENTS

This work was performed in the framework of the Teramobile project, funded jointly by the Deutsche Forschungsgemeinschaft (Germany) and the Centre National de la Recherche Scientifique (France). We acknowledge support from the TLS technical team, especially J. Haupt, A. Kirchhof, M. Pluto, J. Winkler, and help from K. Stelmaszczyk and H. Wille. The Teramobile web site is www.teramobile.org

- [1] A. Braun, G. Korn, X. Liu, D. Du, J. Squier, and G. Mourou, *Opt. Lett.* **20**, 73 (1995).
- [2] J. Kasparian, R. Sauerbrey, and S. L. Chin, *Appl. Phys. B: Lasers Opt.* **71**, 877 (2000).
- [3] A. Becker, N. Aközbeke, K. Vijayalakshmi, E. Oral, C. M. Bowden, and S. L. Chin, *Appl. Phys. B: Lasers Opt.* **73**, 287 (2001).
- [4] N. Aközbeke, A. Iwasaki, A. Becker, M. Scalora, S. L. Chin, and C. M. Bowden, *Phys. Rev. Lett.* **89**, 143901 (2002).
- [5] J. Kasparian, R. Sauerbrey, D. Mondelain, S. Niedermeier, J. Yu, J.-P. Wolf, Y.-B. André, M. Franco, B. Prade, A. Mysyrowicz, S. Tzortzakis, M. Rodriguez, H. Wille, and L. Wöste, *Opt. Lett.* **25**, 1397 (2000).
- [6] J. Kasparian, M. Rodriguez, G. Méjean, J. Yu, E. Salmon, H. Wille, R. Bourayou, S. Frey, Y.-B. André, A. Mysyrowicz, R. Sauerbrey, J.-P. Wolf, and L. Wöste, *Science* **301**, 61 (2003).
- [7] P. Rairoux, H. Schillinger, S. Niedermeier, M. Rodriguez, F. Ronneberger, R. Sauerbrey, B. Stein, D. Waite, C. Wedekind, H. Wille, and L. Wöste, *Appl. Phys. B: Lasers Opt.* **71**, 573 (2000).
- [8] G. Méjean, J. Kasparian, E. Salmon, J. Yu, J.-P. Wolf, R. Bourayou, R. Sauerbrey, M. Rodriguez, L. Wöste, H. Lehmann, B. Stecklum, U. Laux, J. Eislöf, A. Scholz, and A. P. Hatzes, *Appl. Phys. B: Lasers Opt.* **77**, 357 (2003).
- [9] B. La Fontaine, D. Comtois, C. Y. Chien, A. Desparois, F. Gérin, G. Jarry, T. W. Johnston, J. C. Kieffer, F. Martin, R. Mawassi, H. Pépin, F. A. M. Rizk, F. Vidal, C. Potvin, P. Couverture, and H. P. Mercure, *J. Appl. Phys.* **88**, 610 (2000).
- [10] M. Rodriguez, R. Sauerbrey, H. Wille, L. Wöste, T. Fujii, Y.-B. André, A. Mysyrowicz, L. Klingbeil, K. Rethmeier, W. Kalkner, J. Kasparian, E. Salmon, J. Yu, and J.-P. Wolf, *Opt. Lett.* **27**, 772 (2002).
- [11] H. Wille, M. Rodriguez, J. Kasparian, D. Mondelain, J. Yu, A. Mysyrowicz, R. Sauerbrey, J.-P. Wolf, and L. Wöste, *Eur. Phys. J.: Appl. Phys.* **20**, 183 (2002).
- [12] B. La Fontaine, F. Vidal, Z. Jiang, C. Y. Chien, D. Comtois, A. Desparois, T. W. Johnston, J.-C. Kieffer, H. Pépin, and H. P. Mercure, *Phys. Plasmas* **6**, 1615 (1999).
- [13] M. Mlejnek, E. M. Wright, and J. V. Moloney, *Phys. Rev. E* **58**, 4903 (1998).
- [14] A. Couairon and L. Bergé, *Phys. Rev. Lett.* **88**, 135003 (2002).
- [15] M. Mlejnek, E. M. Wright, and J. V. Moloney, *Opt. Express* **4**, 223 (1999).
- [16] M. Mlejnek, M. Kolesik, J. V. Moloney, and E. M. Wright, *Phys. Rev. Lett.* **83**, 2938 (1999).
- [17] P. Sprangle, J. R. Peñano, and B. Hafizi, *Phys. Rev. E* **66**, 046418 (2002).
- [18] H. Schillinger and R. Sauerbrey, *Appl. Phys. B: Lasers Opt.* **68**, 753 (1999).
- [19] A. Proulx, A. Talebpour, S. Petit, and S. L. Chin, *Opt. Commun.* **174**, 305 (2000).
- [20] A. Talebpour, S. Petit, and S. L. Chin, *Opt. Commun.* **171**, 285 (1999).
- [21] J. Yu, D. Mondelain, J. Kasparian, E. Salmon, S. Geffroy, C. Favre, V. Boutou, and J. P. Wolf, *Appl. Opt.* **42**, 7117 (2003).
- [22] S. Tzortzakis, G. Méchain, G. Pantalano, Y.-B. André, B. Prade, M. Franco, A. Mysyrowicz, J.-M. Munier, M. Gheudin, G. Beaudin, and P. Encrenaz, *Opt. Lett.* **27**, 1944 (2002).
- [23] H. Lehmann, URL <http://www.tls-tautenburg.de/telesc.html>
- [24] M. Mlejnek, E. M. Wright, and J. V. Moloney, *Opt. Lett.* **23**, 382 (1998).
- [25] L. Berge and A. Couairon, *Phys. Rev. Lett.* **86**, 1003 (2001).
- [26] A. Braun, G. Korn, X. Liu, D. Du, J. Squier, and G. Mourou, *Opt. Lett.* **20**, 73 (1995).
- [27] E. T. J. Nibbering, P. F. Curley, G. Grillon, B. S. Prade, M. A. Franco, F. Salin, and A. Mysyrowicz, *Opt. Lett.* **21**, 62 (1996).
- [28] A. Brodeur, C. Y. Chien, F. A. Ilkov, S. L. Chin, O. G. Kosareva, and V. P. Kandidov, *Opt. Lett.* **22**, 304 (1997).
- [29] Y. R. Shen, *The Principles of Nonlinear Optics* (Wiley, New York, 1984).
- [30] F. Courvoisier, V. Boutou, J. Kasparian, E. Salmon, G. Méjean, J. Yu, and J. P. Wolf, *Appl. Phys. Lett.* **83**, 213 (2003).
- [31] O. G. Kosareva, V. P. Kandidov, A. Brodeur, C. Y. Chen, and S. L. Chin, *Opt. Lett.* **22**, 1332 (1997).
- [32] J. Zhang, H. Yang, J. Zhang, X. Lu, Y. Li, Y. Li, H. Teng, Z. Chen, Z. Wei, and Z. Sheng (unpublished).
- [33] S. L. Chin, S. Petit, F. Borne, and K. Miyazaki, *Jpn. J. Appl. Phys.* **38**, L126 (1999).
- [34] L. Bergé, S. Skupin, F. Lederer, G. Méjean, J. Yu, J. Kasparian, E. Salmon, J. P. Wolf, M. Rodriguez, L. Wöste, R. Bourayou, and R. Sauerbrey, *Phys. Rev. Lett.* (to be published).
- [35] H. R. Lange, G. Grillon, J.-F. Ripoche, M. A. Franco, B. Lamouroux, B. S. Prade, A. Mysyrowicz, E. T. J. Nibbering, and A. Chiron, *Opt. Lett.* **23**, 120 (1998).
- [36] G. Méjean, R. Bourayou, S. Frey, M. Rodriguez, J. Yu, J. Kasparian, E. Salmon, R. Sauerbrey, L. Wöste, and J.-P. Wolf (unpublished).